quartz crystal, $d_1$ = crystal thickness, approximately 3 millimeters, $Q$ = cavity $Q$, approximately 200 (set), and $\lambda_s$ = sonic wavelength, approximately 1.7 microns.

## Conclusion

Using the semigraphical approach presented previously, it is a relatively simple task to arrive at a satisfactory radial cavity design. Furthermore, once the design has been made, its complete performance and efficiency can then be determined through utilization of the appropriate relations developed herein.

## Acknowledgment

The author is deeply indebted to Prof. J. Lamb and J. H. Collins of the Electrical Engineering Department of the University of Glasgow for encouragement and assistance in the preparation of this and other associated works. The finanical assistance contributed by the National Engineering Laboratory, Ministry of Technology, and the Canadian National Research Council is also gratefully acknowledged.

## References

[1] J. Lamb and H. Seguin, "Measurement of viscoelastic properties of liquids at 3000 Mc/sec," *J. Acoust. Soc. Am.*, vol. 39, pp. 519–526, 1966.
[2] C. G. Montgomery, R. H. Dicke, and W. M. Purcell, Eds., *Principles of Microwave Circuits*, vol. 8, M.I.T. Radiation Lab. Ser. New York: McGraw-Hill, 1948, p. 274.
[3] G. B. Collins, Ed., *Microwave Magnetrons*, vol. 6, M.I.T. Radiation Lab. Ser. New York: McGraw-Hill, 1948, p. 50.
[4] H. Seguin, Ph.D. dissertation, University of London, England, 1963, p. 310.
[5] H. H. Skilling, *Fundamentals of Electric Waves*. New York: Wiley, 1956, p. 89.
[6] C. G. Montgomery et al., *op. cit.*, p. 250.
[7] N. Marcuvitz, Ed., *Waveguide Handbook*, vol. 10, M.I.T. Radiation Lab. Ser. New York: McGraw-Hill, 1951, p. 307.
[8] C. G. Montgomery et al., *op. cit.*, p. 273.
[9] H. Seguin, *op. cit.*, p. 325.
[10] *Ibid.*, p. 327.
[11] M. J. P. Musgrave, "The propagation of elastic waves in crystals and other anisotropic media," *Rep. Prog. Phys.*, vol. 22, pp. 74–96, 1959 (see esp. p. 85).
[12] H. Seguin, *op. cit.*, p. 317.
[13] N. Marcuvitz, *op. cit.*, p. 35.
[14] H. Seguin, *op. cit.*, p. 174.
[15] N. Marcuvitz, *op. cit.*, p. 32.
[16] C. G. Montgomery et al., *op. cit.*, p. 254.
[17] T. Moreno, *Microwave Transmission Design Data*. London: Dover, 1948, p. 215.
[18] *Ibid.*, p. 12.
[19] *Ibid.*, p. 214.
[20] H. E. Bömmel and K. Dransfeld, "Excitation of hypersonic waves by ferromagnetic resonance," *Phys. Rev. Lett.*, vol. 3, pp. 83–84, July 15, 1959.

# Piezoelectric Pulse and Code Generators

OTMAR M. STUETZER, FELLOW, IEEE

***Abstract*—A device technique is discussed, which permits the electroacoustic generation of electrical or of acoustic megahertz pulses or pulse sequences with kilowatt powers. The devices consist of groups of piezoelectrically active elements, separated by acoustic delay lines. A sudden change in applied pressure or electric field generates electrical or acoustic wave trains; they may be programmed to contain information.**

**This paper presents a first order design theory for such piezoelectric pulse train and code generators, with emphasis on arrangements producing electrical output from electrical input. The output depends on the load, and on the geometric arrangement; the latter controls the superposition of responses from the elements. The optimum impedance for a noninductive load is found, and the energy conversion efficiency for this case is estimated; it increases with the number of active elements.**

**Selected experimental devices are described; typically they contain from 4 to 16 piezoelectric elements of 0.01 to 0.1 cm thickness and 5 cm² cross section, generate pulse frequencies from 1 to 10 MHz, pulse trains from 3 to 10 cycles, and code signals of 20 μs duration. Performance limitations are introduced by bonding technology, geometric tolerances, electric breakdown, and circuit inductance.**

Manuscript received September 20, 1966. This work was supported by the United States Atomic Energy Commission.
The author is with Sandia Laboratory, Albuquerque, N. Mex.

### List of Often Used Symbols

| Symbol | Units | Definition |
|---|---|---|
| $A$ | $m^2$ | Electroded area of active element |
| $C$, ($C_s$, $C_p$) | F | Capacitance (of series or parallel circuit) |
| $C_d$ | F | Capacitance of active region = $\epsilon^S A/s(1-k^2)$ or $\epsilon^T A/s$ |
| $c^D$ | $N/m^2$ | Stiffness (at constant flux) $= c_{33}^D$ for axial excitation |
| $D$, $D_1$ | $C/m^2$ | Dielectric flux, "displacement" |
| $\epsilon$, ($\epsilon^S$) | F/m | Permittivity (at constant $S$) |
| $E$, $E_1$, $E^{(1)}$ | V/m | Field strength |
| $g$, $\bar{g}$ | $m^2/C$ | = abbreviation for $h_{33}/c_{33}^D$ or $-h_{31}/c_{11}^D$, respectively |
| $h$ | V/m | $= -(\partial E/\partial S)_D$, $= h_{33}$ for axial and $h_{31}$ for lateral initiation |
| $I$, ($I_s$) | A | Current (short circuit) |
| $k(=k_t)$ | — | Thickness dilatational coupling factor $= h\sqrt{\epsilon^S/c^D}$, $\neq k_{33}$ |

| | | |
|---|---|---|
| $K$ | — | Transmission factor [see (13)] |
| $L$ | V-s/A | Inductance |
| $P$ | C/m$^2$ | Permanent polarization |
| $r$ | — | Reflection coefficient [see (12)] |
| $R$ | V/A | Resistance |
| $s$, ($s_1$, $s_2$) | m | Thickness of sample (initiator, transducer) |
| $S$ | — | Strain |
| $t$, ($t_1$) | s | Time (transit time through active element) |
| $T$, $T_0$, $T_1$ | N/m$^2$ | Stress |
| $v$ | m/s | Acoustic velocity |
| $V$, ($V_{20}$) | V | Voltage (peak voltage for open circuits) |
| $V^*$ | m$^3$ | Volume |
| $W$, ($W_0$) | VA-s = Nm | Energy (energy invested in initiator) |
| $W_{20}$ | VA-s = Nm | First pulse energy in optimum load |
| $Z$, $Z_0$, $Z_1$ | kg/m$^2$-s | Acoustic impedance |

Subscript 1 refers to initiator, subscript 2 to transducer.

## I. Introduction

THE STRONG coupling between acoustic and electric fields in piezoelectric crystals or poled ferroelectric materials has led to efficient electromechanical transducers.[1],[2],[3]

In this paper we consider the performance of multiregime piezoelectric arrangements, energized mechanically or electrically, and initiated by an electrical switch. The distribution of piezoelectric regions and a system of electrodes are chosen in such a way that step excitation produces mechanical or electrical pulse trains, i.e., alternating power, or an information carrying sequence of such pulses.

An example shall introduce our technique. In Figs. 1(a) through 1(d), sets of piezoelectric elements, polarized and electroded as indicated, are excited sequentially by an acoustic stress step $T$ of long duration. For each set of transducers, the open-circuit voltage sequence generated by the transit of $T$ will have the shape of a double sawtooth [Fig. 1(e)]. The combination of Figs. 1(a) and (1b) will produce two such voltage pulses, separated by the travel time of $T$ through the inactive metal line. If not one single stress front $T$, but a sequence of properly spaced extensional and compressional mechanical pulses travel through the transducers of Fig. 1, pulse trains of longer duration and, by superposition, of higher amplitude may be generated.

The arrangements of Fig. 1 can, conversely, be used to generate mechanical stress fronts. If an electric step voltage is applied between a pair of output leads, the piezoelectric parts suddenly expand or contract and a series of acoustic pulses, corresponding to the above electric pulses, will start traveling through the system.

The devices under consideration will combine both electrical and mechanical pulse generation. The output will be an electrical or a mechanical pulse train. An example of practical importance is shown in Fig. 2. A stack of active "initiator" disks [Fig. 2(a)] are electrically charged by an applied field. Every time this is shorted out by a switch, a number (in this example 7) of alternating stress fronts leave the initiator side. Traveling through two groups of active material, this mechanical pulse system will excite electrical pulse groups energizing the load $R_2$. Figure 2(b) shows the wave shape obtained across a high impedance load; the second pulse train is enhanced by acoustic end reflections.

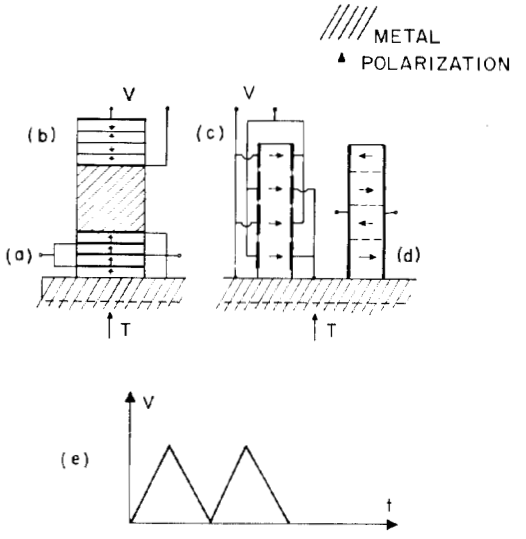


Fig. 1. Stress wave activation of piezoelectric transducer arrangements: (a) and (b) axial; (c) and (d) transverse initiation; (e) open-circuit voltage output. [For arrangement (c) output voltage (e) is idealized.]

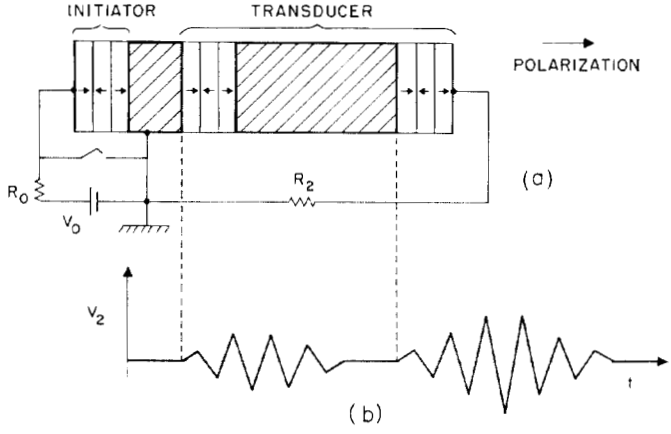


Fig. 2. (a) Electrically driven pulse-train generator, identified later as {[3; 3, 3|} arrangement. (b) First transit open-circuit response.

From Figs. 1 and 2, it is evident that large variations in pulse number, pulse duration, and electrical and mechanical impedances can be obtained by variation of geometry and electrode connections. With ferroelectric ceramic materials, the electrical and acoustical pulse amplitude can, in addition, be modified by varying the degree of polarization. We do not need an electrical battery to generate the initiating field—it can be obtained by compressing mechanically the generator disks, or, if they are ferroelectric, by heating them up.

To develop a design theory for such devices, we shall

treat the basic energy conversion and superposition processes common to all variations. A special example, the axially excited electrical-to-electrical converter of Fig. 2, will be emphasized; it is the arrangement which permits the highest frequency response. We shall ease our analytic problems by assuming the active elements to be thin plates; in every system they shall have the same acoustic length. The analysis will be approximate and restricted to linear dependence of displacement on stress and field increments; i.e., the linearized piezoelectric equations will be used. The theory will, therefore, not cover initiation by explosive shock loading,[2],[3] which promises one-shot megawatt powers; we shall obtain only kilowatt peak outputs, but nondestructively.

The elementary arrangement for generating acoustic pulses is a piezoelectric disk on a semi-infinite wall; Cook[4] has discussed at an early time a graphical solution for its transient response. The simplest generator for electrical pulses consists of two active elements connected by an elastic line; Onoe[5] has given a general description of its performance, emphasizing delay line aspects. For our analysis of multielement devices, a simplified mathematical description will be developed, which permits taking mechanical cascading and electrical load dependence into account easily. The 6 mm or $\infty$ mm piezoelectric symmetry exhibited by poled ferroelectric ceramics will be assumed for detailed calculations; this assumption does not materially affect the results, which are, therefore, quite general.

We shall first analyze the dynamic response of a single active piezoelectric transducer element in a circuit to a mechanical stress front. Then, conversely, the initiation of mechanical pulses by electrical steps will be discussed. Combining the results, we shall investigate the behavior of initiators and transducers connected by a delay line, and derive a useful method for calculating superpositions of multiple excitations. Having thus developed an approximate analysis for a pulse generator, we shall then estimate its energy conversion efficiency for noninductive loads.

Experiments supporting our theoretical findings will be reported next. To convey, at this time, a general idea on the size and shape of experimental devices, Fig. 3 shows a number of models before or after assembly. Their frequency response, determined by the transit time of the acoustic front through the active elements, ranges from 300 kHz (large device in background) to 30 MHz (small structures in foreground). Pulse trains carry up to $10^{-2}$ J of energy into suitable loads.

Finally, the limitations of our device technique will be assessed as they appear at the present state of materials technology.

Applications are not discussed; a number of obvious ones are pointed out by the experiments.

## II. Mechanical Generation of Electrical Pulses

The transient behavior of a piezoelectric disk in a circuit is complicated. Through electromechanical coupling, all

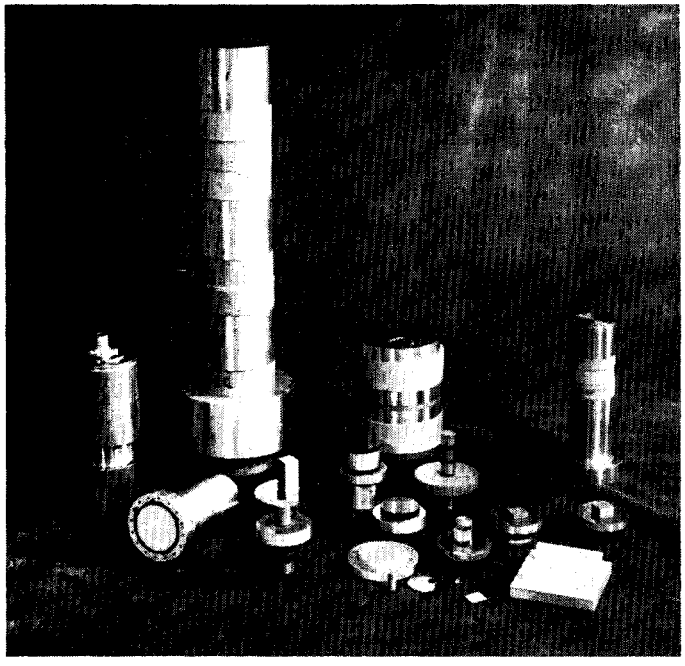

Fig. 3. Generator and transducer models, partly assembled.

acoustic changes affect all electrical changes and vice versa. We shall make a simplifying assumption, which will later be shown to be quite permissible for our purposes: the stress front of amplitude $T$, which traverses the active elements, will be considered unchanged by the interaction. The permittivity $\epsilon$ in the stressed regions of the devices will furthermore, and legitimately so, be assumed the same as in the (temporarily) unstressed regimes.

### A. Axial Excitation (Common D)

With these restrictions we shall compute the power generated in a transducer, when one stress front of amplitude $T$ traverses it axially, as shown in Figs. 1(a) and 1(b). The thin elements are assumed under unidimensional strain. Power generation occurs only while the stress front propagates through transducer material. The analysis of devices like the ones in Fig. 1 is, therefore, made simple by looking only at the piezoelectric element through which the mechanical pulse front travels, and by lumping all the other elements in the system into a capacitance $C'$. The transducer may then work into a resistive, inductive, or capacitive load. Quite general circuits for the operation of the device are, therefore, sketched in Fig. 4(a) (series load) and in Fig. 4(b) (parallel load). The capacitance $C$ includes the above defined inactive capacitance $C'$ of the transducer. The active material is assumed to be a good insulator.

For stress $T$ below the yield strength, no space charges are generated in the active material. The divergence of the dielectric flux or displacement $D$ is then zero, $\nabla \cdot \vec{D} = 0$. If the disks are thin, the problem is a one-dimensional one; it follows that $\partial D/\partial x = 0$ and $D$ is a function of time only.

Following partly Neilson[2] and Anderson,[6] an approximate differential equation for the circuits in Figs. 4(a) and 4(b) is now easily established. For no lateral

TABLE I
RESPONSE OF PIEZOELECTRIC THIN DISK TO STRESS FRONT $T$

| | Series Circuit, Fig. 4(a) | Parallel Circuit, Fig. 4(b) |
|---|---|---|
| Differential Equation | $LI'' + RI' + I/C_s - gTv = 0$<br>where $1/C_s = 1/C + 1/C_d$ | $V'' + V'/RC_p + V/LC_p = 0$<br>where $C_p = C + C_d$ |
| Boundary Conditions | $I = 0$, $I' = 0$ for $t = 0$ | $V = 0$, $V' = gTv/(1 + C/C_d)$ for $t = 0$ |
| | Solutions: $(0 < t \leq s/v)$ | |
| General Solution | $I = gTvC_s\left\{1 - e^{-Rt/2L}\left[\cos \omega t + \frac{R}{2\omega L}\sin \omega t\right]\right\}$ (4s)<br>where $\omega^2 = (1/LC_s) - (R/2L)^2$ | $V = \frac{gTv}{\omega}\cdot\frac{1}{1 + C/C_d}\cdot e^{-t/2RC}\cdot \sin \omega t$ (4p)<br>where $\omega^2 = (1/LC_p) - (1/2RC_p)^2$ |
| Special Case: No Inductance | $I = gTvC_s[1 - e^{-t/RC'}]$; (5s) | $V = gTvRC_d[1 - e^{-t/RC_p}]$ (5p) |

strain and 6 mm symmetry, fields, strains, and stresses in stressed part (1) of Fig. 4(a) are linked by the piezoelectric equations. Using customary notation with 3 as axial direction, we have $T_3 = c_{33}^D S_3 - h_{33}D_3$ and $E_3 = -h_{33}S_3 + D_3/\epsilon_{33}^S$. Eliminating $S_3$ and omitting the subscripts 3 and 33, we find

$$D = \epsilon^S E^{(1)}/(1 - k^2) + \epsilon^S hT/c^D(1 - k^2). \quad (1a)$$

Here, $\epsilon^S$ is the permittivity measured under constant strain, $h = -(\partial E/\partial S)_D$ is a piezoelectric constant, $c^D$ is the open circuit stiffness, and $k(= k_t)$ is the associated coupling factor $h\sqrt{\epsilon^S/c^D}$.

In the "undisturbed" regime (2) in Fig. 4(a) we have $T = 0$ and, therefore,

$$D = \epsilon^S E^{(2)}/(1 - k^2). \quad (1b)$$

The current through the system is given by

$$I = A \cdot dD/dt, \quad (2)$$

where $A$ is the cross-sectional area of the active element.

At time $t = 0$, the pressure front shall enter the active element; it progresses with velocity $v$. The potential at the position of the acoustic wavefront, which in the time $t$ has covered a distance $v \cdot t$, is $-E^{(1)}vt$ [see Fig. 4(a)]. The potential across the whole disk of thickness $s$ is consequently $-E^{(1)}vt - (s - vt)E^{(2)}$. This potential has to oppose the voltage drop across the load. We obtain from (1) and (2), abbreviating $h/c^D = h_{33}/c_{33}^D = g$ (which is not identically equal to $g_{33}$),

$$\frac{dV}{dt} + \frac{I}{C_d} - gTv = 0. \quad (3)$$

The capacitance $C_d = \epsilon^S A/s(1 - k^2)$ is the capacitance of the active element which is laterally clamped by its neighbors. (If, instead of a clamped thin plate, we had considered a long bar, we would have obtained an identical equation (3), but with $C_d = \epsilon_{33}^T A/s$ and $g = g_{33}$.)

Differential equation (3) permits calculations of $I$ or $V$, once the dependence of $I$ on $V$ is furnished. As this is a function of the load only, (3) holds both for the series circuit of Fig. 4(a) and the parallel circuit of Fig. 4(b).

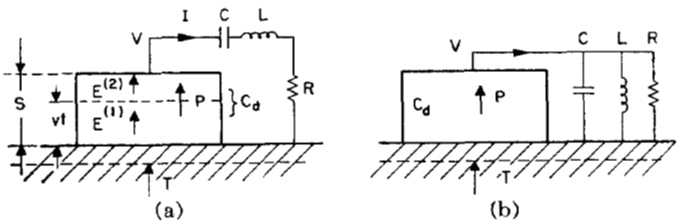


Fig. 4. Axial excitation of thin piezoelectric element by stress front $T$; load is in (a) series and (b) parallel connection.

In Table I the circuit properties of the load have been introduced into (3); for the new circuit equations, the general and a specific solution have been tabulated. With inductance, we obtain the circuit rings with the angular frequency expected from its total capacitance. Without inductance, exponential charge-up behavior determined by capacitance and load resistance. For some special values of the load impedance, the response of the transducer element is plotted in Fig. 5.

Useful for measurements is a relation, which describes the case where the active disk is only loaded by a circuit capacitance. For $L = 0$, $R = 0$ in the series circuit and $L = \infty$, $R = \infty$ in the parallel case we obtain for the voltage across the disk

$$V_d = gTv \cdot t \cdot \frac{1}{1 + C/C_d}, \quad (6)$$

the ramp function illustrated in Fig. 5(d).

### B. Transverse Excitation (Common E)

For lateral application of the energizing stress front, as indicated in Figs. 1(c) and 1(d) and in more detail in Fig. 6, an analysis quite closely corresponding to the one above yields

$$\frac{dV}{dt} + \frac{I}{C_d} - \frac{s}{w}\bar{g}Tv = 0. \quad (7)$$

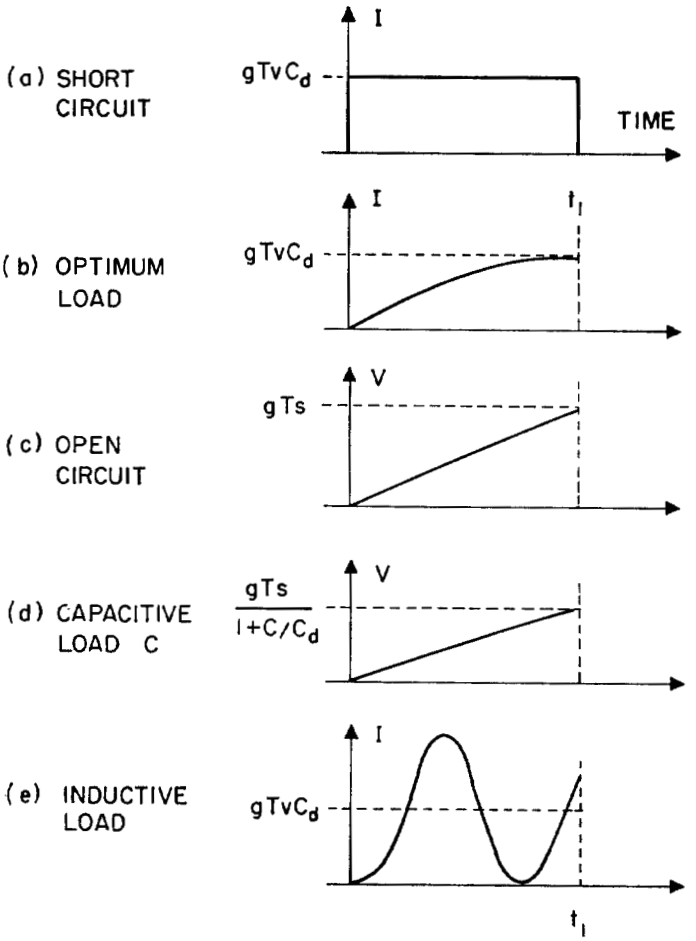


Fig. 5. Output of stress front activated piezoelectric element for special values of load.

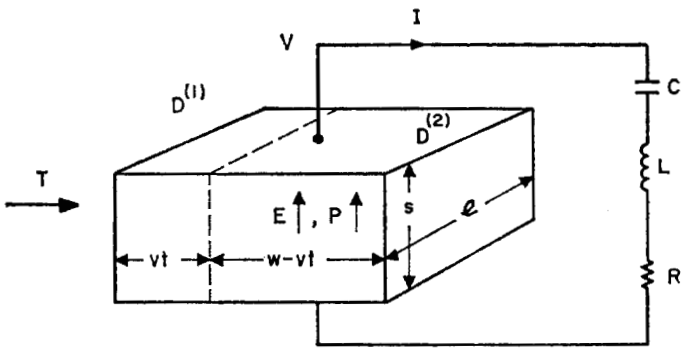


Fig. 6. Transverse mechanical activation of piezoelectric transducer with series load.

For active elements clamped perpendicularly to the direction of stress propagation, we find $\bar{g} = -h_{31}/c_{11}^{D}$, which is a positive quantity. (For the free bar approximation $\bar{g} = -g_{31}$.) Equation (7) is essentially identical with (3). We can, therefore, use all our previous results, if we modify the stress strength by the thickness to width ratio $s/w$.

### C. Quality of Approximation

As stated, the calculations we have made neglect the modification of the stress wave $T$ by the influence of the varying fields in the transducer element. This can be taken into account only by a complete solution of the boundary problem for a stress initiated element. A method to obtain this for axial excitation of thin disks has been published by Redwood.[7] Adapted to our case,[8] the detailed calculations reveal the following.

For open circuit operation the solutions presented above are rigorous.

Our short-circuit expression (equation (5) with $R = 0$) predicts constant current, i.e., $I_s = gTvC_d$. The accurate solution introduces a time variation which depends on the associated coupling factor $k$ of the material and also on mechanical boundary conditions (which our approximation does not). For a thin disk between two line elements of the same acoustic characteristic impedance, e.g., the short-circuit current is modified by a factor $\exp(k^2t/t_1)$; for a reflecting end disk the factor is $\exp(3k^2t/2t_1)$. Here, $t_1 = s/v$ is the transit time through the element. The quantity $k^2$ is, for present materials, smaller than 0.25.

We rarely operate devices in short-circuit condition, however, but will mostly use an optimum load to extract a maximum of energy. For this the deviation from the correct solution turns out to be never more than 15 percent for present materials, and the average deviation is about half of this value. For devices which contain only a few active elements, the approximation presented is therefore well acceptable; for arrangements with a large number of elements we have to be cautious.

The nonlinear field dependence of the displacement $D$ and the stress $T$, important for the approach of Wittekindt[9] and Halpin,[3] can be and is neglected for the pressure range which we consider.

## III. Electrical Generation of Mechanical Pulses

Sudden changes of an electric field $E$ in a piezoelectric element produce mechanical stress fronts. With proper circuits, fields can be changed so fast that the electrical phenomena have ended before the acoustic events have noticeably developed. This simplifies the mathematical analysis. A complication is introduced by the need to consider both electrical and mechanical boundary conditions simultaneously. We shall discuss two extreme situations for the electrical exciting circuit, infinite and zero impedance.

### A. Charge-Up Excitation (Constant D)

Assume a thin region of thickness $s_1$ within a slab of material of identical acoustic impedance, bounded by ideal (i.e., acoustically noninterfering) parallel electrodes (Fig. 7). The region shall be polarized in the indicated direction. An electric generator shall suddenly apply a field $E_1$ which generates a charge $D_1A$; then the generator shall present an infinite impedance to the circuit.

At the moment of application, the active plate is inertially clamped by the adjoining material; the charge density on the electrodes is therefore $D_1 = \epsilon^S E_1$, with $\epsilon^S = \epsilon_{33}^S$, and the subscript 1 not inferring a directional notation. By definition the rise time of the charge pulse was so short that strain in the material could not develop.

TABLE II
FIRST PULSE TRANSMISSION FOR ACOUSTIC MATCH, $K = 1$, SERIES CIRCUIT TRANSDUCER, AND IDENTICAL INITIATOR AND TRANSDUCER MATERIALS

| We apply | | Transmitted stress $T_1$ | Short-circuit current $I_{2s}$ | Max. open-circuit voltage $V_{20}$ | Invested energy $W_0$ | Optimum first step efficiency $W_{20}/W_0$ |
|---|---|---|---|---|---|---|
| Field $E_1$ | Suddenly | $\frac{h\epsilon^S E_1}{2}$ | $\frac{k^2}{2} vE_1C_s$ | $\frac{k^2}{2} E_1 s$ | $\frac{\epsilon^S}{2} E_1^2 V^*$ | $\frac{.1k^4}{1-k^2}\cdot\frac{C_s}{C_d}$ |
| | Slowly, then compensate | $-\frac{h\epsilon^S E_1}{2(1-k^2)}$ | $-\frac{k^2}{2(1-k^2)} vE_1C_s$ | $-\frac{k^2}{2(1-k^2)} E_1 s$ | $\frac{\epsilon^S}{2(1-k^2)} E_1^2 V^*$ | $\frac{.1k^4}{(1-k^2)^2}\cdot\frac{C_s}{C_d}$ |
| | Slowly, then short-circuit | $-\frac{h\epsilon^S E_1}{2}$ | $-\frac{k^2}{2} vE_1C_s$ | $-\frac{k^2}{2} E_1 s$ | $\frac{\epsilon^S}{2(1-k^2)} E_1^2 V^*$ | $.1k^4\cdot\frac{C_s}{C_d}$ |
| Stress $T_0$ | Slowly, then short element | $\frac{k^2 T_0}{2(1-k^2)}$ | $\frac{k^2}{2(1-k^2)} gvT_0C_s$ | $\frac{k^2}{2(1-k^2)} gT_0 s$ | $\frac{1}{2c^D} T_0^2 V^*$ | $\frac{.1k^6}{(1-k^2)^3}\cdot\frac{C_s}{C_d}$ |

$C_s$ = stack capacitance
$s$ = element thickness
$v$ = sound velocity
$C_d$ = single element capacitance
$A$ = element area
$V^*$ = element volume

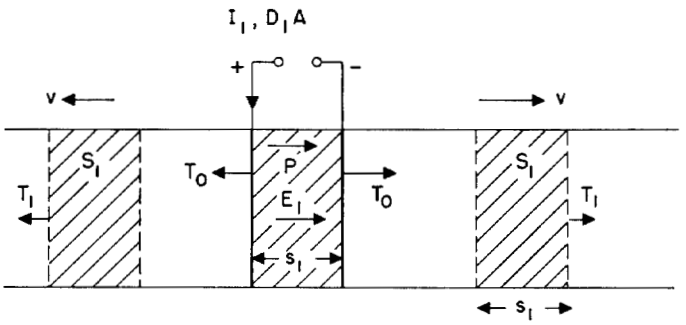


Fig. 7. Electrical step initiation of piezoelectric element in matched line generates two stress pulses.

A stress $T$ has been generated, however. With strain $S = 0$, the piezoelectric equations yield for its axial component $T_0 = -hD_1 = -h\epsilon^S E_1 = -eE_1$, with the subscript 33 omitted.

The element behaves now exactly as if it had suddenly been placed under axial stress $T_0$. As we have stipulated infinite circuit impedance, or constant $D$, the electric circuit does not interfere with the acoustic phenomena developing. At each boundary, a stress front of amplitude $T_1$ propagates inward, a relief front $-T_1$ outward. The two fronts pass through one another and follow the outward going relief fronts. Hence, an initial electrical step results in two rectangular stress pulses as indicated in Fig. 7. The energy balance of the situation reveals that $T_1 = T_0/2$. We have, therefore, generated two mechanical pulses with the amplitudes

$$T_1 = h\epsilon^S E_1/2 = eE_1/2, \tag{8}$$

and both of duration $s_1/v = t_1$.

### B. Discharge Excitation (Constant D)

Assume the active element is first charged up slowly and clamped laterally. It has time to strain axially and will, therefore, accept a charge density $D_1 = \epsilon^S E_1/(1-k^2)$, which is higher than in the previous example. We now suddenly remove the charge $D_1$ by, e.g., depositing a countercharge $-D_1$ through an ideal spark gap, which shall immediately assume a high resistance again. With an argument analogous to the above, it is found that we have now generated stress pulses of amplitude

$$T_1 = -h\epsilon^S E_1/2(1-k^2) = -eE_1/2(1-k^2). \tag{9}$$

(If the element is originally unclamped, a charge density $D_1 = \epsilon^T E_1$ will be accumulated. Its sudden compensation generates a propagating stress $T_1 = -h_{33}\epsilon_{33}^T E_1/2$.)

### C. Short Circuit (Constant E)

Consider the active plate charged up slowly as in the last example, but now suddenly short-circuited permanently, as in Fig. 2. Now the initial strain $S_0 = h\epsilon^S E_1/c^D(1-k^2)$, in collapsing, will set up currents in our circuit and generate charges on the electrodes which will make the relief pulse amplitude a function of time, similar to the situation discussed above for the short-circuit current. In the first instant, the amplitude of the pulse will be

$$T_1 \approx -h\epsilon^S E_1/2 = -eE_1/2. \tag{10}$$

This value will be adopted as an approximation.

A practically interesting variation of short-circuit initiation is obtained by addition of an inductance, which smoothes the mechanical pulses and can increase their amplitude. Its mathematical analysis is too lengthy to be considered here. Of interest are also nonelectrical methods of energization. Static or dynamic stresses, or, for ferroelectric transducers, heat[10] can be utilized to generate the field $E_1$, which may then be collapsed by a switch. In Table II, more fully discussed below, we have for comparison added energization by unidimensional static stress $T_0$ to the above discussed cases.

The above derivations and comments pertain to axial propagation of the generated stress pulses; all piezoelectric and dielectric constants should therefore be taken with

a 33 subscript. It can be seen that lateral stress pulse generation [e.g., in an arrangement like Figs. 1(c) or 1(d)] is covered by replacing $e_{33}$ and $h_{33}$ through $e_{31}$ and $h_{31}$, but leaving $\epsilon_{33}^S$ and $\epsilon_{33}^T$ unchanged.

## IV. The Two-Element Pulse Generator

Having investigated acoustoelectric generators and electroacoustic transducers, we will now briefly discuss the simplest combinations of these elements. Attenuation losses in the connecting lines will be neglected. As active parts and lines are not necessarily made of the same materials, the acoustic characteristic impedance $Z$ of the components will have to be taken into account.

The "initiator," i.e., the acoustic generator will be identified by subscript 1, and the acoustoelectric transducer by 2. We will simplify our task greatly by choosing all transducer plates or disks of the same acoustic length, i.e., the transit times $s_1/v_1 = s_2/v_2 = t_1$ shall be the same.

The simplest case is sketched in Fig. 8. A voltage $V_1 = |s_1 E_1|$ will be applied. With idealized charge-up excitation and no step in characteristic impedance, i.e., $Z_0 = Z_1$, a stress pulse $T_1 = h\epsilon^S V_1/2s_1$ [see (8)] would leave the acoustic generator at initiation time traveling towards the transducer. If $Z_0$ is of general value, $T_1$ is known to be modified by a factor

$$1 + r_{10} = \frac{2Z_0/Z_1}{1 + Z_0/Z_1}, \tag{11}$$

where $r_{10}$ is the reflection coefficient:

$$r_{10} = \frac{1 - Z_0/Z_1}{1 + Z_0/Z_1}. \tag{12}$$

A corresponding modification occurs at the entry into the transducer 2, and we obtain for the first stress pulse $T_2$ which traverses the transducer

$$T_2 = T_1 \cdot \frac{4Z_2/Z_1}{(1 + Z_0/Z_1)\cdot(1 + Z_2/Z_0)} = KT_1. \tag{13}$$

This defines a transmission factor $K$. We may modify $K$ by an absorption term, if we desire to take acoustic attenuation along the delay line into account. Of course, $T_2$ may be higher than $T_1$.

Knowing $T_2$, the electrical response of the transducer 2 can now be found from the equations of Table I. The output depends on the load selected.

For the short-circuit current $I_{2s}$, we obtain in transducer time $t$ from (8), (13), and (5s) with $R = 0$, the relation:

$$\frac{I_{2s}}{V_1} = K \cdot \frac{k_1^2}{2} \cdot \frac{c_1^D}{c_2^D} \cdot \frac{h_2}{h_1} \cdot \frac{v_2 C_{2d}}{s_1}, \qquad 0 < t \leq t_1. \tag{14}$$

For open-circuit operation, the secondary voltage will rise linearly to a maximum value $V_{20}$ determined by

$$\frac{V_{20}}{V_1} = K \cdot \frac{k_1^2}{2} \cdot \frac{c_1^D}{c_2^D} \cdot \frac{h_2}{h_1} \cdot \frac{s_2}{s_1}, \qquad 0 < t \leq t_1. \tag{15}$$

(Subscripts 33 have been omitted. The equations hold also for lateral instead of axial initiation, if $h_{31}$ and $c_{11}^D$ values are used and $k^2$ is replaced by $-\epsilon_{33}^S h_{31}^2/c_{11}^D$.) The

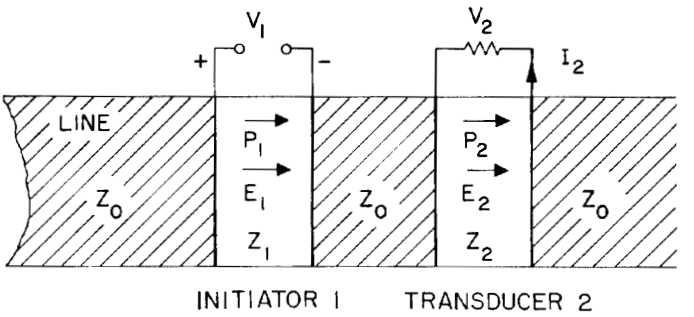


Fig. 8. Combination of initiator and transducer on elastic line.

above equations simplify obviously, if we use the same active material for both transducers. Changing the method of electrical initiation may change the responses (14) and (15) by a small factor (see Table II). To obtain the responce with a general loading circuit, we have to use (4s) or (4p) from Table I in combination with (8) or (9), and (13).

The importance of the coupling factor $k$ is made evident by (14) and (15). The value of $k$ can, for ferroelectrics, be controlled electrically within a wide range. Its maximum is about 0.5. The transmission coefficient $K$ is close to unity for a reasonable acoustic match; in practical cases the ratio $c_1^D h_2/c_2^D h_1$ is also close to one.

We have, so far, described the response of our system for the first transit on the transducer side, $0 < t \leq t_1$. After this time quite complex phenomena may occur. The dominant effect is due to the fact that the stress pulse (Fig. 7) has by definition the duration $t_1$, and now its rear enters the transducer 2. If no reflections take place in the system, i.e., if $Z_0 = Z_1 = Z_2$, the pressure simply returns progressively to zero. The short-circuit current (14) just reverses. The open-circuit voltage (15) drops linearly to zero. This situation is illustrated in Fig. 9, which will be discussed in more detail shortly.

If an acoustic mismatch is present, multiple reflections occur, i.e., pulse sequences will be generated in our device.[5] This phenomenon could be used to generate pulse trains. We shall, however, discuss a more efficient and controllable way to do so, which involves the use of sequences of active elements.

## V. Multielement Arrangements

The general response of a device like the one in Fig. 8, but containing several initiator and converter elements (see Fig. 2) and working into an LRC circuit, is quite complicated. We would have, e.g., to superimpose with proper time delay a number of expressions of the type given in (4s) or (4p), Table I, adding ringout contributions. Fortunately, for a number of technically interesting designs, and for open- or short-circuit operation, the behavior of multielement pulse generators can be much more easily described. The simplification we shall make at first is to choose the characteristic impedances of the active devices equal, $Z_1 = Z_2 = Z$, and the impedance of the line either equal to this value, $Z_0 = Z$, or zero. The latter stipulation means a totally reflecting end.

The three possibilities for one disk arrangements are sketched in Fig. 9. We see that open end reflections generate additional superimposed pulses, which make the responses longer and tend to increase the center amplitudes of the pulse trains. Adding more elements in proper phase relationship rapidly enhances this effect.

A rather simple algebraic scheme makes it possible to calculate the response of an arrangement like the one in Fig. 2:

a) *Initiators* are characterized by the pulse fronts they *transmit* towards the transducer. We designate a tensile stress front $\delta T$ by a unity symbol 1, and a compressive front by $\bar{1}$. We write sequences of these symbols, with neighboring elements representing conditions at intervals of one transit time $t_1$. The total number of pulse fronts transmitted is obtained by algebraically adding, at the correct time, our unity stress symbols. A single disk in between two matching lines (Fig. 9, top) is therefore, designated $1\ \bar{1}$; a reflecting end disk (Fig. 9, center) or two matched reversed disks have the symbol

$$\begin{array}{r} 1\ \bar{1} \\ +\ \bar{1}\ 1 \\ \hline 1\ \bar{2}\ 1 \end{array},$$

and so forth. As an example to which we shall return later, we have shown in Fig. 10 an arrangement of three active disks, separated by two inactive regions of equal acoustic lengths, and with one end totally reflecting. Its code symbol is found to be $1\ \bar{1}\ 1\ \bar{1}\ 1\ \bar{2}\ 1\ \bar{1}\ 1\ \bar{1}\ 1$. The stress front sequence corresponding to this is sketched. Its integral in time is of course the acoustic response of the arrangement.

b) On the *transducer* side, the same symbolic notation is used to characterize the sequence and sign of *transits*. A tensile front transit is marked by 1, a compressive transit by $\bar{1}$. A reflecting end plate element is, therefore, characterized by $1\ \bar{1}$.

Each unit pulse front transit generates a unit current pulse in a short-circuited transducer. Amplitude and sign sequence of resulting pulse trains is, therefore, simply obtained by algebraic multiplication of the symbols. As shown, a two end-disk code arrangement (see Fig. 9, bottom) will generate a current pulse sequence

$$\begin{array}{r} 1\ \bar{2}\ 1 \times 1\ \bar{1} = 1\ \bar{2}\ 1 \\ \bar{1}\ 2\ \bar{1} \\ \hline 1\ \bar{3}\ 3\ \bar{1} \end{array}.$$

The open-circuit voltage sequence, as can be seen, may be determined by integrating the current response. For our algebraic symbolism, this is easily done: starting with a zero, we add the current symbols cumulatively. For the current sequence $1\ \bar{3}\ 3\ \bar{1}$ of the last example (Fig. 9, bottom), we obtain $0\ 1\ \bar{2}\ 1\ 0$ this way.

The method furnishes, of course, only relative current or peak voltage values of subsequent pulses. This is sufficient, however, as the absolute values of the first pulse have been obtained above. Table II lists them for several ways of initiation.

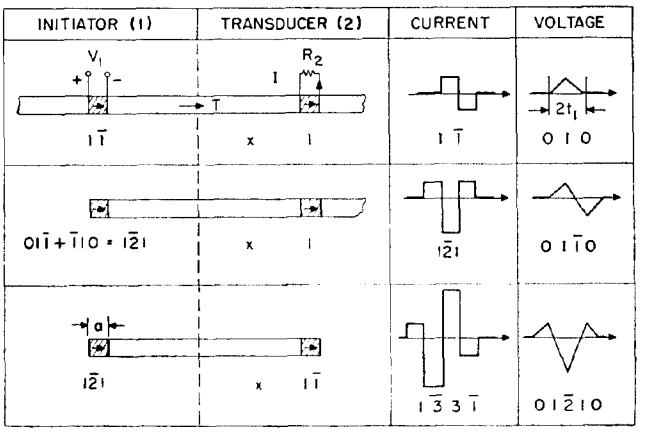


Fig. 9. Simple pulse generators and their electrical response upon electrical initiation. From top to bottom: {1; 1}, {|1; 1}, and {|1; 1|} arrangement. Direction of output current and voltage is drawn for charge-up initiation.

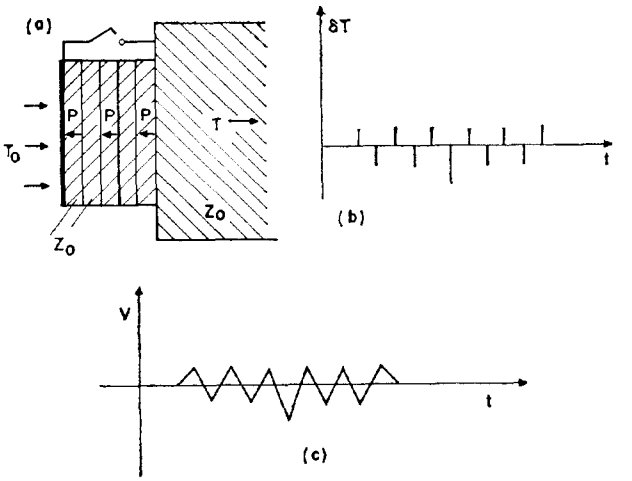


Fig. 10. Mechanical pulse generator energized by stress $T_0$ and initiated by electrical switch. (a) Arrangement; (b) mechanical pulse fronts generated; (c) electrical response of pressure gauge.

For simple multidisk arrangements, the symbolism leads to rather easily remembered pulse sequences. Let us, e.g., consider $N$ successive reversely poled (or circuit reversed) disks both for transmitter and receiver.

If one of the two ends is reflecting, the other one matched to a reflectionless line (equivalent to Fig. 9, center), we shall designate this arrangement as an $\{|N; N\}$ generator. (The bar | indicates the acoustically reflecting end.) The sequence of short-circuit pulses generated by this arrangement, irrespective of which end we choose as initiator, is:

Sequence $\{|N; N\}$

$$= 1\ \bar{3}\ 5 \cdots (2N-1), \underbrace{2N, 2N, \cdots, 2N}_{N\text{times}}, (2N-1), \cdots \bar{5}\ 3\ \bar{1}.$$

The relative sign of the first pulse with amplitude $2N$ is $(-1)^N$.

If both ends of the above arrangement are made totally reflecting, we obtain a $\{|N\ ;\ N|\}$ device with the response:

Sequence $\{|N; N|\}$

$$= 1\ 3\ 5 \cdots \overline{(4N-1)},\ (4N-1), \cdots \bar{5}\ 3\ \bar{1},$$

yielding a total of $4N$ pulses.

TABLE III
SIMPLE CODE SEQUENCES WITH REFLECTIONS, ALGEBRAIC PRESENTATION

| | Code | Response after indicated multiples of transit time $t_1$: 1 | 2 | 3 | 4 | 5 | 6 | 7 | 8 | 9 | 10 | 11 | 12 |
|---|---|---|---|---|---|---|---|---|---|---|---|---|---|
| CURRENT | $\{\|1;1\|\}$ | 1 | $\overline{3}$ | $3-2r$ | $\overline{1-6r}$ | $\overline{6r}$ | $2r$ | | | | | | |
| | $\left\{\begin{matrix}\|1;2\| \\ \|2;1\|\end{matrix}\right\}$ | 1 | $\overline{3}$ | $4-r$ | $\overline{4-3r}$ | $3-5r$ | $\overline{1-7r}$ | $\overline{7r}$ | $5r$ | $\overline{3r}$ | $r$ | | |
| | $\{\|2;2\|\}$ | 1 | $\overline{3}$ | 5 | $\overline{7}$ | $7-2r$ | $\overline{5-6r}$ | $3-10r$ | $\overline{1-14r}$ | $\overline{14r}$ | $10r$ | $\overline{6r}$ | $2r$ |
| VOLTAGE | $\{\|1;1\|\}$ | 0 | 1 | $\overline{2}$ | $1-2r$ | $4r$ | $\overline{2r}$ | 0 | | | | | |
| | $\left\{\begin{matrix}\|1;2\| \\ \|2;1\|\end{matrix}\right\}$ | 0 | 1 | $\overline{2}$ | $2-r$ | $\overline{2-2r}$ | $1-3r$ | $4r$ | $\overline{3r}$ | $2r$ | $\overline{r}$ | 0 | |
| | $\{\|2;2\|\}$ | 0 | 1 | $\overline{2}$ | 3 | $\overline{4}$ | $3-2r$ | $\overline{2-4r}$ | $1-6r$ | $8r$ | $\overline{6r}$ | $4r$ | $\overline{2r}$ |

The symbolism developed permits the prediction of pulse sequences generated by rather complex structures. It can be refined in many ways. As elements may be intentionally poled to different degrees (or over different areas), the stress pulses or the electrical pulses generated may have different amplitudes from disk to disk. We can take this into account by not assigning unity strength 1 or $\bar{1}$, but variable amplitudes $A_n$, $\bar{A}_m$ to the respective disks.

For evaluating experimental results, another refinement is needed: we assumed in the above discussion either total or no reflection. The latter condition is often hard to meet between transmission line and active regions. Now multiple reflections have to be followed through the system by means of "ray tracing". Power series of the reflection coefficient $r$ (12) enter our algebraic scheme. With practice, simple sequence laws quickly become evident. While straightforward, the method is too cumbersome to discuss here. We shall bring a few results, however. In Table III, the response of reflecting end pulse generators is shown. Symbol $\{|1;1|\}$ designates the arrangement of Fig. 9, bottom. The $\{|2;1|\}$ and $\{|1;2|\}$ generators have two initiator or two transducer disks, respectively; their responses are identical. The $\{|2;2|\}$ generator has two elements at each end.

Figure 11 illustrates the open-circuit voltage response of a symmetric $\{|2;2|\}$ generator with the reflection coefficient $r$ between active elements and line as parameter. The dashed trace is the ideal response, $r = 0$. It is seen that for positive reflection coefficients (i.e., line impedance higher than element impedance) a sign reversal occurs after the fifth peak.

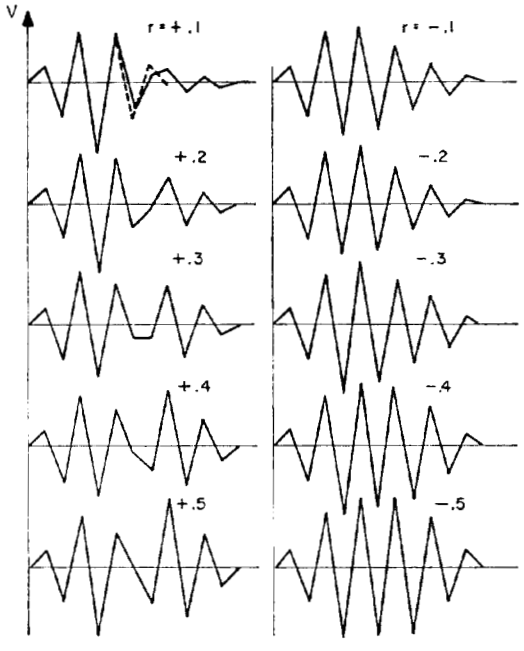


Fig. 11. Response of an electric to electric $\{|2;2|\}$ generator with positive and negative reflection coefficient $r$ between active material and connecting line.

## VI. Energy Conversion Efficiency

For most applications it will be of importance how much energy can be extracted by an ohmic load $R_2$ immediately after initiation, i.e., without multiple reflections in the system. We may call this the "first transit" efficiency. To estimate it, we shall a) compute the conversion efficiency obtained on transit of the first stress pulse through the first transducer element and then b) extend the result to pulse trains.

a) The conversion efficiency in the transducer depends, of course, strongly on the choice of the load $R_2$. We shall restrict this to an inductance free series circuit; the capacitance $C_s$ is or includes the series capacitance of the active elements. During the first pulse front transit the energy collected by the load $R_2$ (Fig. 4a) will then be, with (5s) of Table I,

$$W_2 = (g_2 T_2 v_2 C_{2s})^2 R_2 \int_0^{t_1} [1 - \exp(-t/R_2 C_{2s})]^2 \, dt. \quad (16s)$$

Evaluation of (16s) shows that $W_2$ has a broad maximum $W_{20}$ in the vicinity of

$$R_{20} \approx \frac{t_1}{2C_{2s}}, \tag{17s}$$

which is, therefore, the optimum load (it can be seen that it is the optimum load not only for the first step, but for any transit).

With this, the maximum value of $W_2$ is found to be

$$W_{20} \approx 0.19(g_2T_2)^2 s_2^2 C_{2s}. \tag{18s}$$

Introduction of $T_2$ from (13) and (5s) of Table I, and division by the invested energy $W_0 = \epsilon^s E_1^2 A s_1/2$, leads to the optimum first step energy transfer ratio

$$\frac{W_{20}}{W_0} \approx \frac{.1K^2k_1^2k_2^2}{(1-k_2^2)} \cdot \frac{c_1^D}{c_2^D} \cdot \frac{s_2}{s_1} \cdot \frac{C_{2s}}{C_{2d}}. \tag{19s}$$

Again, this expression simplifies considerably for use of identical materials on both sides of the generator. For this latter situation, and $K = 1$, the ratio $W_{20}/W_0$ has been listed in Table II for several methods of excitation; it is approximately proportional to $k^4$ for electrical and to $k^6$ for mechanical energization.

For the parallel circuit of Fig. 4(b), (17s) and (19s) have to be modified. The optimum load is now calculated to be

$$R_{20} \approx \frac{t_1}{2C_{2p}}, \tag{17p}$$

and the maximum first step efficiency is:

$$\frac{W_{20}}{W_0} \approx \frac{.1K^2k_1^2k_2^2}{(1-k_2^2)} \cdot \frac{c_1^D}{c_2^D} \cdot \frac{s_2}{s_1} \cdot \frac{C_{2d}}{C_{2p}}. \tag{19p}$$

If we can neglect circuit capacitances not contributed by the active disks, the ratios $C_{2s}/C_{2d}$ and $C_{2d}/C_{2p}$ are just equal to $1/N$ for $N$-disk transducer arrangements. The values for $W_{20}/W_0$ are about $5 \times 10^{-3}/N$ with PZT ceramics.

b) We proceed now to the discussion of the energy conversion efficiency for a total pulse train. To avoid forbidding mathematical complications, we have to be satisfied with an estimate.

From Fig. 9 we know, say for a $\{|1;\,1|\}$ reflecting end generator, the short-circuit current and the open-circuit voltage response. For the optimum load $R_{20}$, the response lies between the two, as indicated in Fig. 12. In Fig. 13 the instantaneous power has been plotted versus time. The four power pulses are slightly shifted in phase with respect to the transit time steps. Integrating graphically, we recognize that their energy ratio is nearly $1:9:9:1$, i.e., the square of the current pulse ratio. It was found that this approximation is quite reasonable for other sequences, if they are not too long (i.e., contain less than 15 elementary pulses).

As the energy in the first pulse is known from (19s) or (19p), the energy delivered by the pulse train can now be estimated. We shall, as an example, express it for an $\{|N;\,N|\}$ generator, i.e., a symmetric arrangement, with open reflecting ends:

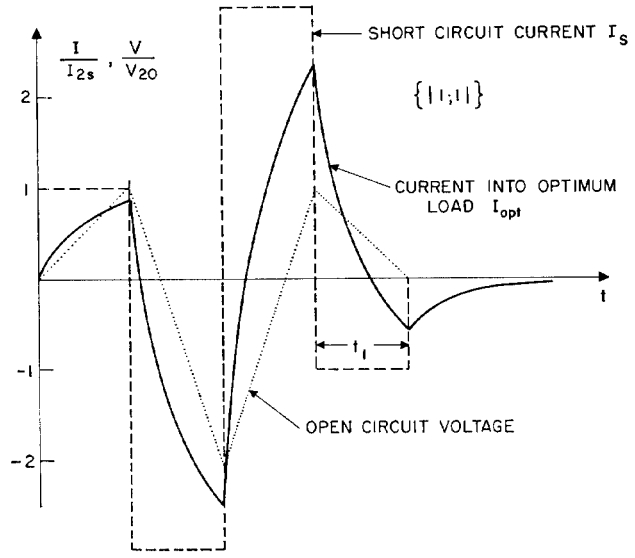


Fig. 12. Theoretical optimum load response of $\{|1;\,1|\}$ generator compared to short-circuit and open-circuit output.

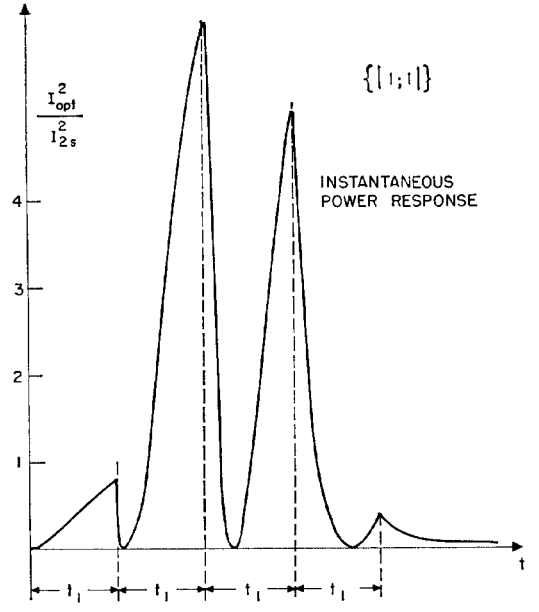


Fig. 13. Instantaneous power output of $\{|1;\,1|\}$ generator into optimum ohmic load.

If the input energy is $W_0$ for one element, it is $W_{0\,tot} = N \cdot W_0$ for $N$ elements.

The output energy for optimum load is $W_{20}$ in the first pulse; for the current sequence $[1:3:5 \cdots (4N-1) \cdots]$ derived above, the energy steps will, therefore, be $1:9:25 \cdots$, and the total energy will be

$$2 \cdot W_{20} \cdot [1 + 3^2 + 5^2 + \cdots (4N-1)^2] = (4/3) \cdot N \cdot (16N^2 - 1) \cdot W_{20}.$$

The pulse train conversion efficiency is, therefore,

$$\frac{W_{20tot}}{W_{0tot}} \approx \frac{4}{3} \cdot (16N^2 - 1) \cdot \frac{W_{20}}{W_0}, \tag{20}$$

where $W_{20}/W_0$ is found in (19s) or in Table II and is inversely proportional to $N$. The result is the same for transducers in parallel circuit. The usefulness of (20) is

limited to situations where the value $W_{20\,tot}/W_{0\,tot}$ is less than 0.25. Our assumption, that the stress waves are constant during the transit, has to break down with appreciable energy transfer—after all, the energy comes from the stress waves.

We have not considered the influence of a tuning inductance. We shall briefly comment on its improving influence later. Also neglected was acoustic attenuation, which can be quite easily taken into account by appropriate exponential attenuation terms.

## VII. Experiments

A comprehensive program demonstrated that for a wide range of conditions the above theory can be well applied to the design of devices. The active elements used were mostly circular disks from 5 to 50 mm diameter and 0.10 to 25 mm thickness; for axial excitation, the latter dimensions cover frequencies varying from 0.1 to 30 MHz. The active material was quartz, tourmaline, lithium metagallate, but mostly one of the many lead zirconate–titanate compositions (PZT).[11] Outputs expected and obtained varied from watts to kilowatts peak power, energies per pulse train from $10^{-5}$ to $10^{-2}$ J.

### A. Technology

The manufacturing of satisfactory multidisk devices proved far from easy. The main technological problem is presented by the bonds.

Useful bonding materials have a low dielectric constant, a low acoustic impedance, and a low sound velocity compared to, say, PZT. The low dielectric constant makes the capacitance $C_s$ (see Table I) small, and the low $Z$ causes internal reflections. If the bond could be made infinitely thin, these side effects would be negligible. One micron bond thickness is, however, not always easy to obtain with 20 mm diameter disks. With PZT 65–35, a one side epoxy bond of this thickness lowers the eigencapacitance $C_d$ of a 0.075 mm disk with 37 mm diameter from 6300 pF to $C_s$ = 4900 pF and introduces a reflection factor $r$ of about six percent.

Especially annoying acoustically are wedge-shaped bonds between the disks. Due to the low velocity of propagation of the bonding material, sometimes lowered by air bubbles, the wave fronts acquire considerable tilt, which leads to ineffective acoustic fronts.[3]

These phenomena, all escalating with multidisk devices, have to be minimized by extreme mechanical accuracy. The necessary flatness has to be achieved by painstakingly lapping together neighboring active and separating regions. The binder has to be applied in an extremely thin layer. The whole device has then to be pressed in a suitable jig. For epoxy joints a pressure of around 200 atmospheres is recommended. Curing of micron thin epoxy layers takes at least 48 hours; for about a week the bonds still improve somewhat. Only after this time should the devices be exposed to high strain.

Conductive bonds, with, e.g., silver loaded epoxy resins, are more difficult to make well than normal joints. The arrangement of Fig. 1(a), which needs conductive bonds, was therefore avoided when feasible.

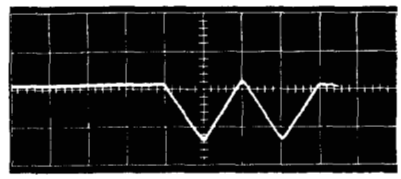

Fig. 14. Open-circuit voltage across four alternately reversed quartz disks, initiated by shock front. Abscissa: 1 μs/unit. Ordinate: 5 V/unit.

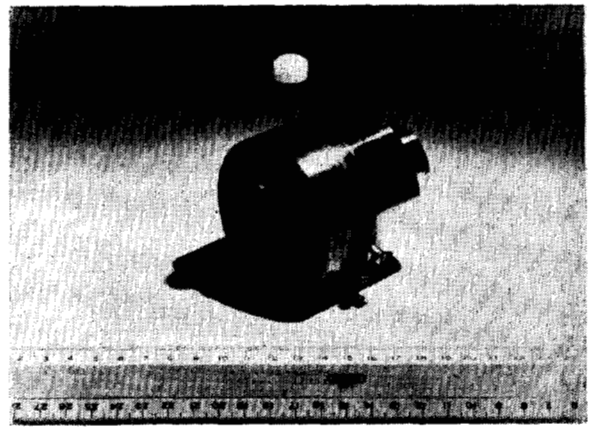

Fig. 15. Mechanically energized mechanical pulse front generator; 3000 V spark gap visible on side.

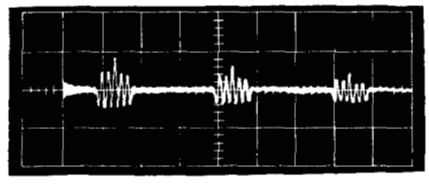

Fig. 16. Pressure gauge reading generated by arrangement 15. Abscissa: 1 μs/unit. Ordinate: 25 V/unit.

### B. Measurements

A number of methods were used to test our devices. A 2 m long helium shock tube of 50 mm diameter was initiated by pressure rupturing of mylar diaphragms of various thicknesses. After calibration with quartz gauges, it was employed to check (5s) of Table I, and (6). Figure 14 illustrates the transit of a single shock front through four alternately reversed quartz disks as drawn in Fig. 1(b). Amplitude and shape are within a few percent of prediction (6).

Mechanical pulse sequences from mechanical energy were, e.g., generated with a device (Fig. 15) which contains the arrangement sketched in Fig. 10(a) and a hydraulic pump to apply pressure $T_0$. The switch is a spark gap, visible on the outside of the pressure vessel. Operation of the Morse key-like pump stem produced the mechanical pulse fronts predicted by Fig. 10(b). This is evidenced by the electrical response (Fig. 16) of a single active element bonded to the end of the acoustic line, which shows exactly the pulse shape of Fig. 10(c), repeated twice by reflections between the boundaries of

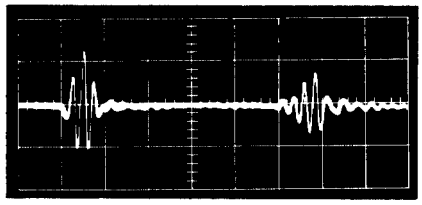

Fig. 17. First and second response of {2; 2'} pulse generator, consisting of 0.75 mm PZT-4 disks. Abscissa: 1 μs/unit. Ordinate: 1 V/unit.

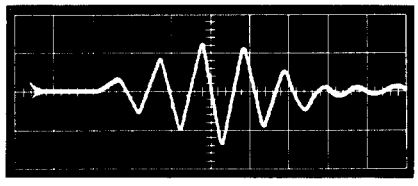

(a)

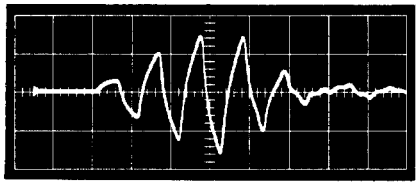

(b)

Fig. 18. (a) Open circuit and (b) optimum load output of {3; 3|} device. Initiated voltage 500 V. Abscissa: 0.5 μs/unit. Ordinate: 50 V/unit for (a) and 20 V/unit for (b).

the system. A peak electrical power of 15 watts could be drawn.

Electrical energization and electric readout were most often utilized on account of simplicity and fast repeatability. The initiator was either suddenly connected to a charged-up cable or it was charged up slowly over a high resistor and then suddenly short-circuited. Some devices of this type were already introduced in Fig. 3.

Figure 17 illustrates the response of a {|2; 2|} code as analyzed in Fig. 11, but with a reflection factor $r = 0.07$. It was obtained by charging the double disk transmitter to 13 volts and then short-circuiting it. Inserting measured values of $C_s$ into (15), we expected the first pulse to reach 0.38 volt; Fig. 11 (top, left) then tells us that the signal should later reach three times this value. The measurement yielded 1.2 volts. The expected "phase reversal" is observed, as we see. (The trace shows also the shape of the pulse after it has been reflected again through the system. The distortions observed, e.g., a small precursor, can be very well accounted for by an extension of our analysis.)

Figure 18 shows the effect of loading. Open-circuit response of a {|3; 3|} arrangement is compared with the response into the optimum load.

For high power, i.e., high strain operation, it is advantageous to contain the devices by a cage under, say, 200 atmospheres of static pressure. This assures long life of the bonds—in $10^7$ operations no noticeable deterioration was observed with a variety of materials. Figure 19 shows models; they contain arrangements similar to Fig. 2,

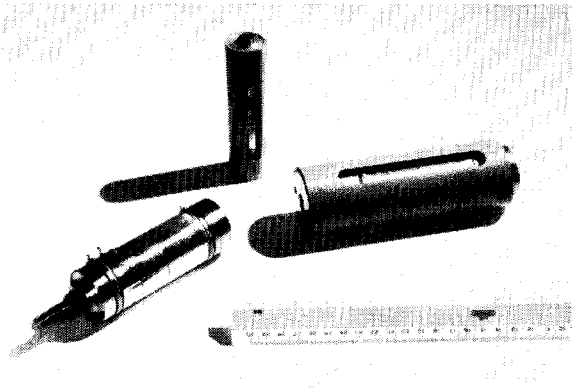

Fig. 19. Mechanical containment of generators: centerbolt prestressed device (left) together with external cage generators.

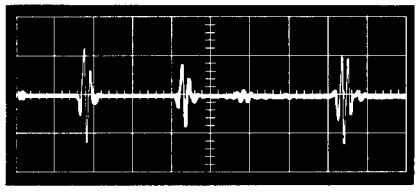

Fig. 20. Information bearing {|2; 1, 1, 2|} code generator. Abscissa: 2 μs/unit. Ordinate: 200 V/unit.

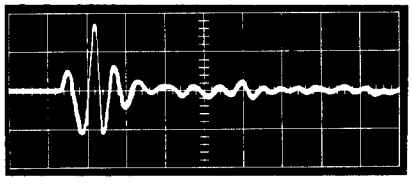

Fig. 21. High power {|2; 2|} generator energized by 6 kV. Abscissa: 2 μs/unit. Ordinate: 500 V/unit.

but outfitted with low $Z$, i.e., well reflecting end plates for mechanical connection with the cage.

Figure 20 presents the response of a {|2; 1, 1, 2|} information bearing code generator: two counterpoled initiator disks generate a mechanical pulse system, which activates successively two single disks and a double element, spaced in desired distances. A "ghost" response, due to imperfect match, is visible. Peak output power was about 400 watts into 150 ohms. The device, otherwise closely similar to Fig. 2, was initiated by a spark gap at a kilohertz pulse repetition rate.

Some devices with kilowatt peak power were built and tested. The highest power obtained was observed with a {|2; 2|} generator, made of 37.5 mm PZT-4 disks, which furnished 14.5 kW into a 50 ohm load. The output (shown in Fig. 21) was somewhat marred by multiple reflections due to nonideal bonds.

The response of a {|8; 8|} generator is traced in Fig. 22. Absorption in the bonds and the material caused the peak voltage to be 30 percent lower than the superposition calculation in Section VI predicts.

Up to now, none of the described experiments contained any inductance other than the unavoidable one of the circuit. While unrewardingly complex analytically, the addition of a suitable inductance will, of course, lengthen and smooth out our generated pulses, and can excite

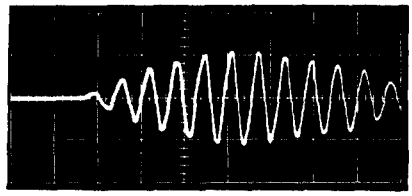

Fig. 22. {|8; 8|} generator, consisting of 0.75 mm PZT disks, and energized by 500 V, working into 80 Ω load. Abscissa: 0.5 μs/unit. Ordinate: 20 V/unit.

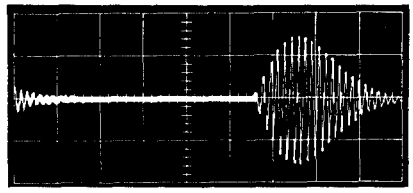

Fig. 23. Effect of tuning: {|3; 3|} generator made of 0.125 mm tourmaline disks and tuned to 30 MHz. Abscissa: 0.2 μs/unit. Ordinate: 50 V/unit. Load was 430 Ω.

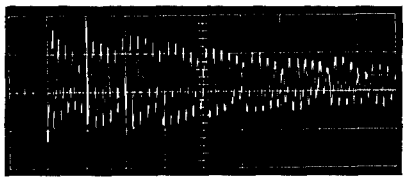

Fig. 24. PZT-4 {|1; 1|} generator with very short separating line, tuned to fifth harmonic of acoustic response. Abscissa: 0.5 μs/unit. Ordinate: 1 V/unit.

harmonics. It will also improve the match to the load and, therefore, increase power output, especially for longer pulses. The improvements, depending on the loaded $Q$ of the circuit, can be estimated with standard circuit theory. Figure 23 shows the first response of a {|3; 3|} tourmaline generator tuned electrically to its acoustic frequency, 30 MHz. The length of the pulse is extended by about a factor 3, compared to the {|3; 3|} code of Fig. 18. Figure 24, finally, records the response of a {|1; 1|} code with a very thin wall between initiator and transducer. The acoustic response is 2 MHz, and the system is electrically tuned to its fifth harmonic.

## VIII. Limitations of the Technique

Although many aspects and possibilities of electroacoustic pulse generation have not been discussed, the developed state of the art permits an assessment of the limitations of the technique.

The transit time $t_1 = s_1/v$ determines the main frequency component of the generated signal, $f = 1/2t_1 = v/2s$. A practical limit for grinding single crystal material like quartz or tourmaline seems to be 5 microns thickness, leading to a limiting frequency of 600 MHz for quartz. In theory we may, by adding a proper inductance, let the device ring in a third or higher harmonic and obtain a higher frequency at a sacrifice in power.

With ferroelectric ceramics a natural limitation is the grain size of the materials, presently 10 microns or more. If ground to a thickness below that limit, the material properties change. This produces a frequency limitation of about 200 MHz. Relaxation phenomena may depress this value to one half, if large signal changes are desired.[12] Power limitation at high frequencies, due to the high permittivity of these materials, is discussed below.

A low frequency limitation is given by the weight and size of the devices. A 10 kilocycle PZT element would have to have one dimension of about 150 mm.

A serious power bound is presented by the limiting field strength $E_b$ of our materials. This may be the breakdown or the depoling field strength. It prevents us from building up voltages higher than $E_b s$ and sometimes forces us to abandon desired high impedance loads. The maximum power obtainable from any similar device is (stored energy/release time)

$$\dot{W}_{max} \approx \frac{\epsilon E_b^2}{2} \cdot A \cdot v, \tag{21}$$

where $\epsilon$ is the applicable dielectric constant. For present ferroceramics, about $3 \times 10^7$ W/m$^2$ may be expected in the linear regime. For elements in a circuit a capacitance ratio must be added to (21), e.g., $C_s/C_d$ for series circuits.

Constraints are placed on the device designer by the fact that optimum loads $R_{20}$ depend on the capacitance $C_d$ of the active elements (17) and with it on the frequency $f$ selected; so does the inductance $L$ to tune the elements. The variations are substantial; with constant area $A$ the element capacitance $C_d$ is proportional to $f$, and the optimum load $R_{20}$ varies as $f^{-2}$. While series or parallel connection can adjust the optimum load value by a factor of $N$ or $1/N$ for $N$ elements, quite often a device using a certain active material is difficult to match to a prescribed load. The tuning inductance $L$, varying with $f^{-3}$, rapidly assumes rather low values for PZT. For very high frequencies, $L$ approaches the wiring inductance, and tuning to a harmonic becomes impossible.

Another limitation is related to this latter point. It occurs most poignantly when short-circuiting a charged initiator is used to energize the system. The inductance of the short-circuit $L$ is hard to get below the circuit $L \approx \mu R^*$, where $\mu$ is the permeability of vacuum and $R^*$ is the radius of the disk, $R^* = (A/\pi)^{1/2}$. Upon short-circuiting, the disk will ring on with an angular frequency $\omega$, where $\omega^2 LC_d \approx 1$. The acoustic pulse will have a corresponding time constant $t^*$ and will not generate efficiently frequencies higher than $1/t^*$. Some algebra shows that to avoid this we have to select, for one element initiators,

$$R^* \leq \frac{s}{\pi} \cdot \sqrt[3]{\frac{c^2}{\epsilon_{rel} v^2}}, \tag{22}$$

where $\epsilon_{rel}$ is the relative dielectric constant of the element and $c$ is the velocity of light. By limiting the element area, the phenomenon limits the available power at high frequencies, especially for high $\epsilon$ ceramics.

All of our devices are of course microphonic. Any mechanical vibration will produce a disturbing electrical signal. For high-frequency generators, this disadvantage is academic, as sharp enough acoustic fronts do not exist in nature.

Our derivations were limited to "thin" single elements, i.e., unidimensional strain. The connecting lines certainly are not always thin, however. A rounding of the mechanical step front has, therefore, to be expected. While the deviations observed with rather "long" codes (about four times the diameter) turned out to be gratifyingly small, efficiency losses increasing with the transit time through the system will eventually become noticeable.

## IX. Conclusion

A novel technique to produce short pulses or code sequences by piezoelectric energy conversion has been discussed. The analysis emphasized electrical output generation from electrical input. A number of modifications and a variety of applications, not all expressly discussed, are obvious.

Fundamentally, the devices consist of piezoelectric thin elements with varying circuit connections and/or direction of polarization, connected by delaying elastic lines and excited by one or more electrical or mechanical step fronts. The electrical and mechanical pulse generation properties of this arrangement were investigated analytically, using the linearized piezoelectric equations.

A symbolic algebraic method was developed to determine the behavior of multielement arrangements. The "first transit" energy conversion efficiency was estimated and found to increase with the number of converter elements; it depends strongly on the electromechanical coupling factor of the active material.

A large number of experiments showed that the analysis describes our technique to a good approximation. The code frequencies demonstrated were in the lower megacycle regime. Peak powers obtained in nondestructively-initiated devices were several kilowatts. Tuning brought expected advantages.

The method is limited as far as frequency and power generation are concerned, but the limits are quite wide. The main and general advantage of ensuing devices may be seen in simplicity, ruggedness, radiation hardness, and reliability.

## Acknowledgment

The author acknowledges valuable discussions with many members of the technical staff of Sandia Corporation, especially E. P. Eer Nisse, R. W. Holland, C. E. Land, F. W. Neilson, E. L. Patterson, and R. H. Plumlee.

## Bibliography

[1] W. P. Mason, *Piezoelectric Crystals and Their Application to Ultrasonics*. Princeton, N. J.: Van Nostrand, 1960.

[2] F. W. Neilson, "Ferromagnetic and ferroelectric one-shot explosive-electric transducers," *Bull. Am. Phys. Soc.*, vol. 2, p. 302, 1957.

[3] W. J. Halpin, "Current from a shock loaded ferroelectric disk," *J. Appl. Phys.*, vol. 37, pp. 153–163, January 1966.

[4] E. G. Cook, "Transient and steady-state response of ultrasonic piezoelectric transducers," *IRE Conv. Rec.*, vol. 4, pt. 9, pp. 61–69, 1956.

[5] M. Onoe, "Theory of ultrasonic delay lines for direct-current pulse transmission," *J. Acoust. Soc. Am.*, vol. 34, pp. 1247–1254, September 1962.

[6] G. W. Anderson, Sandia Lab., Albuquerque, N. Mex., private communication.

[7] M. Redwood, "Transient performance of a piezoelectric transducer," *J. Acoust. Soc. Am.*, vol. 33, pp. 527–536, April 1961.

[8] O. M. Stuetzer, "Laplace transform analysis of thin piezoelectric plate configurations," Sandia Corp., Albuquerque, N. Mex., Research Rept. 67–66, February 1967.

[9] R. H. Wittekindt, "Shape of the current output pulse from a thin ferroelectric cylinder under shock compression," Diamond Ordnance Fuze Labs., Rept. TR-922, May 1961.

[10] S. R. Hoh, "Conversion of thermal to electrical energy with ferroelectric materials," *Proc. IEEE*, vol. 51, pp. 838–845, May 1963.

[11] H. Jaffe and D. A. Berlincourt, "Piezoelectric transducer materials," *Proc. IEEE*, vol. 53, pp. 1372–1386, October 1965.

[12] R. H. Plumlee, "Pulse poling and switching of polycrystalline ferroelectrics and $BaTiO_3$ crystals," *Bull. Am. Phys. Soc.*, vol. 10, p. 1121, 1965.